High strength and ductile high solid solution AleMg alloy processed by a novel hard-plate rolling route

Min Zha [a], Xiang-Tao Meng [a], Hong-Min Zhang [a], Xuan-He Zhang [a], Hai-Long Jia [b], Yan-Jun Li [b], Jun-Yu Zhang [a], Hui-Yuan Wang [a, *], Qi-Chuan Jiang [a]

[a] Key Laboratory of Automobile Materials, Ministry of Education, and School of Materials Science and Engineering, Jilin University, No. 5988 Renmin Street, Changchun, 130025, PR China
[b] Department of Materials Science and Engineering, Norwegian University of Science and Technology, 7491, Trondheim, Norway

Abstrac

Achieving bimodal grain structure via cold rolling remains a challenge for AleMg alloys. In the present work, a high tensile strength (~525 MPa) and ductile (~14%) Ale9Mg alloy was fabricated by a novel hard-plate rolling (HPR) route with a single-pass thickness reduction of 75%. Increasing solute Mg content promotes a bimodal structure and a high dislocation density in the HPRed AleMg alloys due to the severely retarding effect of Mg solutes on dynamic recovery/recrystallization. The simultaneous high ductility and strength is due mainly to the strong work hardening ability deriving from the bimodal grain structure and the high solute Mg content.

1. Introduction

Developing high strength AleMg alloys with considerable ductility has been a major research focus in the last decade due to the promising combination of strength and ductility [1]. Different approaches have been proposed to improve the general poor ductility of high strength Al alloys, including designing a bimodal grain structure distribution [2], introducing precipitates by aging [3,4], generating nano-twins [5,6], controlling boundary characteristic [4,7]. However, the latter three strategies listed above are not applicable for non-age hardening AleMg alloys. In contrast, a

bimodal grain structure strategy has been demonstrated to be a feasible route in achieving high-strength ductile binary AleMg alloys. In our previous work, a bimodal Ale7Mg alloy consisting of

both coarse micron-sized grain and ultrafine grains (<500 nm) processed by room temperature equal channel angular pressing (RT-ECAP) showed a simultaneous high strength (tensile strength ~507 MPa) and ductility (uniform elongation ~11%) [2]. It is well known that the increased Mg content in Al-Mg alloys can enhance the multiplication of dislocations and suppress dynamic recovery and recrystallization during severe plastic deformation (SPD), which promotes grain refinement and formation of an inhomogeneous microstructure [8,9]. However, it is nearly impossible to

process high solid solution AleMg alloys (with Mg >5 wt.%) more than 3 passes by RT-ECAP without cracks. Therefore, there is a strong need to develop a new route for fabricating hard-to-deform

high Mg content AleMg alloys with a high strength but no sacrifice in ductility.

Conventional rolling has been applied widely in fabricating high strength ultrafine grain sized AleMg alloys at large scales, but the poor formability becomes the burning problem [10]. The large shear stress along rolling direction (RD) during conventional rolling usually results in easier cracking. For this reason, conventional rolling usually resorts to multi-pass with a small reduction per pass,

which results in difficulty in achieving a bimodal grain structure. In contrast, we propose a novel hard-plate rolling (HPR) route, i.e. with two hard plates added to the upper and lower surfaces and

then rolled simultaneously [11], which is demonstrated to be an appropriate choice to process hard-to-deform high solid solution AleMg alloys, where the single-pass thickness reduction can reach

~75% without edge cracking. Therefore, the present study might be the first to realize a large single-pass thickness reduction in an Ale9Mg alloy at RT by utilizing HPR (Ale1Mg and Ale5Mg alloys

were also included for comparison). Interestingly, the HPRed Ale9Mg alloy displays both good ductility and high strength, and the responsible mechanisms are discussed in terms of the

microstructural evolution beings dependent on the Mg solute content and the novel HPR processing route.

Table 1
Chemical compositions of the Al–Mg alloys (wt.%).

Materials	Mg	Fe	Mn	Si	Al
Al–1Mg	1.05	0.06	0.001	0.08	In balance
Al–5Mg	5.37	0.06	0.003	0.04	In balance
Al–9Mg	8.74	0.05	0.004	0.05	In balance

Al-9Mg alloy at RT by utilizing HPR (Al-1Mg and Al-5Mg alloys were also included for comparison). Interestingly, the HPRed Ale9Mg alloy displays both good ductility and high strength, and

the responsible mechanisms are discussed in terms of the microstructural evolution beings dependent on the Mg solute content and the novel HPR processing route.

2. Experimental procedure

The AleMg materials used in this study were melted in an electric resistance furnace with commercial pure Al (99.90%) and pure Mg (99.85%) at ~700 C. The chemical compositions of all alloys measured by an optical spectrum analyzer (ARL 4460, Switzerland) are shown in Table 1. Before HPR, the AleMg alloys were homogenized for 3 h at 580 °C (for Ale1Mg and Al-5Mg alloys)

and 500 °C (for Al-9Mg alloy), followed by water quenching. Average grain sizes of the three starting materials were found to be in the range of ~385 mm for Ale1Mg alloy, ~250 mm for Al-5Mg

alloy and ~200 mm for Ale9Mg alloy, respectively. The added hard plates are made of hardened steel with the size of 1 x 50 x 150mm3 and Rockwell hardness of ~50. The samples were

HPRed to 1.4 mm (thickness reduction of 75%) by one pass at RT. Samples for tensile tests and microstructural characterizations were cut from the central area of the HPRed sheets, parallel to RD.

Transmission electron microscopy (TEM, JEM-2100F, Japan) were operated at 200 kV. Specimens for TEM observations were firstly ground to ~80 mm in thickness and then prepared by ion milling for

~5 h at 5 kV. The ultrafine grain size distributions were measured from ten TEM micrographs for about 80 individual grains for each alloy. For electron backscattered diffraction (EBSD) analysis, specimens were treated by mechanical grinding and then electropolished in a solution of 5% HClO4 and 95% C2H5OH at 20 V for 60-80 s. EBSD characterization was performed with 20 kV acceleration

voltage, 18 mm working distance, 70 ° tilt, and with 0.5 mm scan steps. To relieve the great stress concentration and improve the quality of the Kikuchi patterns, a low-temperature annealing (200-250 °C for 30-60 min) was carried out for Al-5Mg and Al-9Mg alloys. Their Vickers hardness (Hv) values decrease slightly (~15 Hv), which indicates that only weak dislocation recovery

occurred and hence the EBSD results can roughly represent the HPRed structures. X-ray diffraction (XRD, Model D/Max 2500PC Rigaku, Japan) measurements were performed at a scanning rate of

1 °C min using filtered Cu-Ka radiation (l ¼ 1.5406 Å) from a source operating at 30 mA and 40 kV. Tensile tests were carried out by a material testing system (MTS, 810 testing machine) at RT using a

strain rate of 5 x 10^{-4} s^{-1}. Tensile samples have a gauge length of 10 mm and a width of 4 mm. Five parallels for each samples were carried out to obtain consistent stress-strain curves.

3. Results and discussion

Engineering and true stress-strain curves of the ashomogenized and HPRed AleMg alloys are shown in Fig. 1. With increasing Mg content, there is no obvious differences in the uniform

ductility for as-homogenized AleMg alloys while the yield strength (YS) and ultimate tensile strength (UTS) increase gradually. After HPR, however, not only the YS and UTS but also the uniform elongation increases simultaneously. Another interesting phenomenon is that dynamic strain aging (DSA) serrations appear in Al-5Mg and Al-9Mg but not in Ale1Mg, which means that an appropriate amount of solute atoms are necessary to interact dynamically with the mobile dislocations. In the early stage of the tensile tests, the curves are smooth because Mg atoms diffuse slowly and cannot induce DSA effect. When increased to a critical strain (ε_c), i.e. the waiting times (t_w) of dislocations at obstacles are larger than the diffusion times (t_d) of solutes towards or along dislocations, and serrated yielding show up [12]. The ε_c tends to be delayed with high Mg content in Al alloys while the serration amplitude (Dsmax) is enhanced (Fig. 1b). As the mobility of Mg clusters are strongly hindered due to the higher dislocation density resulted by a high solute Mg content (see the microstructure analysis later), the diffusion rate become lower and td become longer, thus a larger ε_c is required to initiate DSA. Meanwhile, a larger stress is required to activate the pinned dislocations and hence Dsmax increases with increasing Mg content. Notably, the HPRed Al-9Mg displays a high strength (UTS ~525 MPa), a high yield strength (YS ~355 MPa) and good ductility

(elongation to failure, df ~14%) simultaneously. Compared with some representative SPD Al-Mg alloys, e.g. an ECAPed Al-7Mg alloy (equivalent strain is 3) which exhibited an UTS ~507 MPa and d_f ~11% [2], while an Ale6Mge0.3Sc alloy subjected to hot-ECAP to 8 passes [13] exhibited a good ductility but a lower UTS of ~389 MPa, the present HPRed Ale9Mg alloy possesses quite impressive tensile properties.

Table 2
The lattice parameter (a), the difference of lattice parameter (Δa) and the loss of Mg concentration (ΔMg) in solid solution determined from XRD patterns of the Al−Mg alloys in as-homogenized and HPRed conditions.

Alloys	State	a (Å)	Δa (Å)	ΔMg (wt.%)
Al−1Mg	as-homogenized	4.0555 ± 0.0001	0.0029	0.54
	as-HPRed	4.0526 ± 0.0002		
Al−5Mg	as-homogenized	4.0805 ± 0.0001	0.0019	0.37
	as-HPRed	4.0786 ± 0.0006		
Al−9Mg	as-homogenized	4.1025 ± 0.0001	0.0079	1.52
	as-HPRed	4.0946 ± 0.0003		

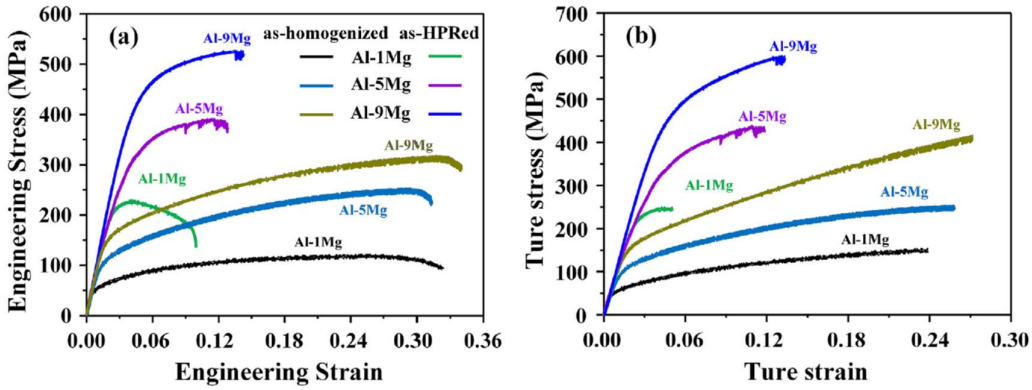

Fig. 1. (a) Engineering and (b) true stress-strain curves of the as-homogenized and HPRed Al–Mg samples, respectively.

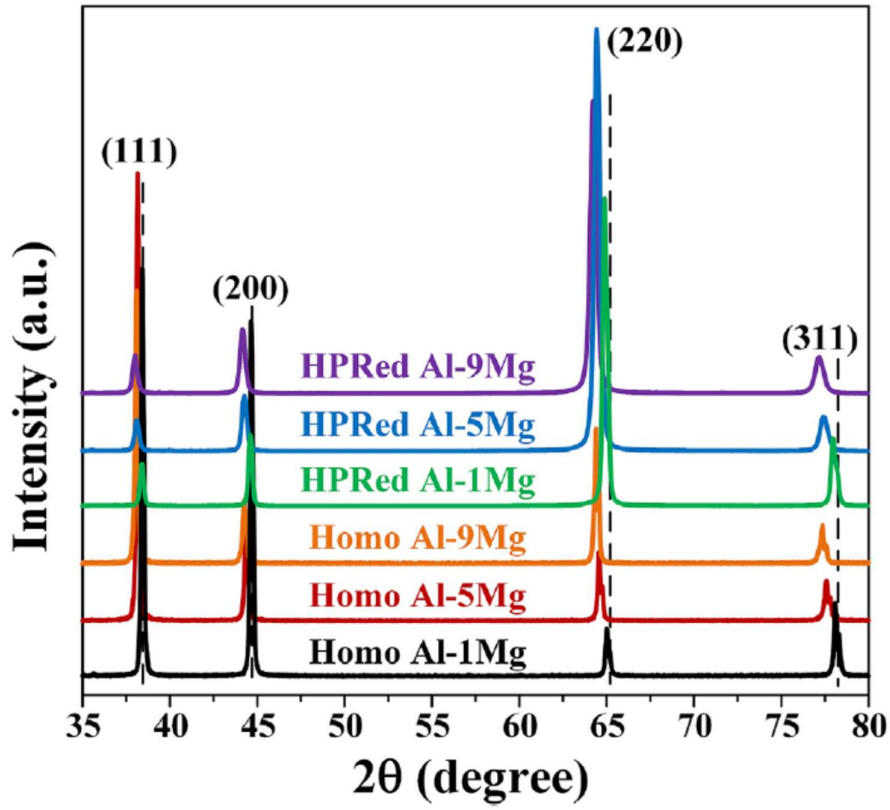

Fig. 2. XRD patterns for (a) the as-homogenized and (b) HPRed Al–Mg alloys, respectively.

Fig. 2 shows XRD patterns of the as-homogenized and HPRed conditions, respectively. For comparison, the theoretical diffraction peaks of pure Al are represented by the vertical dashed lines. For all samples, only diffraction peaks of pure Al were observed and no other precipitates, such as Al3Mg2, could be identified, indicating that most of the Mg atoms are in solid solution. The lattice parameters of the HPRed samples are smaller as compared to their as homogenized counterparts (Table 2). As the solid solubility of Mg in Al is ~11 wt.% at 500 °C , we assume that all Mg atoms are dissolved into the matrix after homogenization at 500-580 °C for 3 h. Actually, the minor difference (Da z 0.002-0.008 Å) between as homogenized and HPRed conditions suggests that the major part

of Mg atoms is retained in solid solution after HPR. The lattice parameter of Al-Mg alloys increases linearly with the amount of Mg in solid solution (1 at.% Mg resulting in a change of a by 0.0046 nm) [14]. Accordingly, the loss of Mg solid solute concentrations in Ale1Mg, Al-5Mg and Ale9Mg samples after HPR are estimated to be 0.54, 0.37 and 1.52 wt.%, respectively. The marginal Mg (DMg) loss might be due to the formation of solute clusters at grain boundaries [15,16].

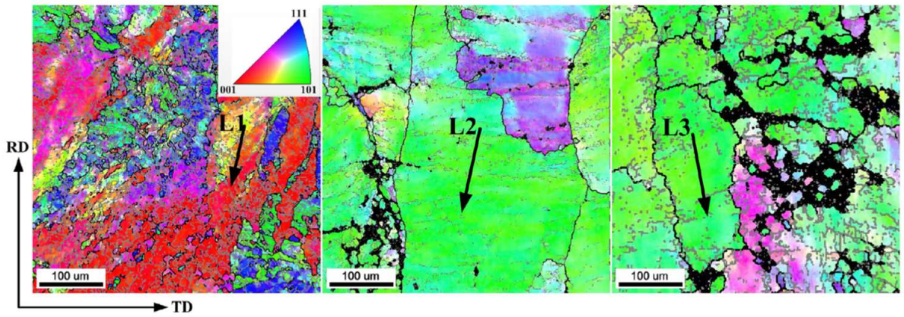

Fig. 3. Typical EBSD maps of (a) Al–1Mg, (b) Al–5Mg, (c) Al–9Mg alloys processed by HPR, respectively, where high-angle boundaries are defined by a misorientation of $\theta > 15°$, and low-angle boundaries are defined by $5° < \theta < 15°$, respectively. The unit triangle inserted in Fig. 3a denotes the crystallographic orientations.

Fig. 3 shows EBSD microstructures of HPRed AleMg alloys. For Al-1Mg alloy, the microstructure is predominated by (001) and (111) oriented grains (Fig. 3a), where deformation bands with (101)

orientations bounded by high angle boundaries are observed and many subgrain structures are frequently seen in the grain interiors. It indicates that extensive deformation already has occurred in the Ale1Mg alloy; however, the initial grains are hardly refined to submicron-scale. As for Ale5Mg and Ale9Mg alloys, the microstructures are dominated by (101) oriented grains (Fig. 3b and c). Jin

et al. reported that four slip systems could be activated simultaneously in the (101) oriented grains in Al-7Mg alloy produced by dynamic plastic deformation (DPD) to the strain of 0.97 at RT,

leading to a homogeneous dislocation distribution, which further promoted these grains to be oriented favorably to accommodate strains [17]. With higher strain, subgrains would rotate progressively to help accommodating the deformation strains, and thus coarse (101) oriented grains are gradually refined into numerous smaller deformation bands and/or sub-structures with (001) and (111) orientations due to fast dynamic recovery, like in the Al-1Mg alloy. However, a high content of Mg solutes in Al matrix increases significantly the critical stress for dislocation slip and hence retards subsequent grain subdivisions. Hence such coarse (101) oriented grains in the Al-5Mg and Al-9Mg alloys, once formed, are relatively stable as compared to the Ale1Mg alloy. Therefore, after HPR processing, a stable microstructure with less (001) and (111) oriented substructures is retained in the Al-5Mg and Al-9Mg alloys. Note that although volumes of different orientations, i.e. (001) and (111) orientations, can also be observed in Al-5Mg and Al-9Mg alloys, these fragmented

volumes are relatively coarse (>100 mm), containing few sub boundaries, and can hardly be further refined, due to the fact that the high Mg content suppresses dynamic recovery. In contrast, the (001) and (111) oriented grains developed in Al-1Mg alloy are usually unstable due to the faster dynamic recovery, and hence more refined subgrain structures are observed in Al-1Mg alloy. Nevertheless, it is difficult to get Kikuchi patterns from areas dominated by fine grains in the HPRed alloys containing

a high Mg content. Even in regions dominated by coarse grains, one can see considerable unidentified areas (black areas) of poor Kikuchi patterns resulting from the extremely fine grain sizes and high solute Mg content (Fig. 3c).

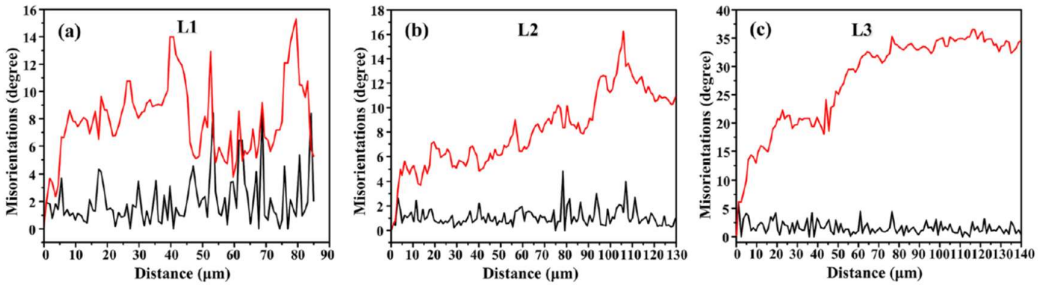

Fig. 4. Corresponding misorientation profiles measured along lines L1–L3 in Fig. 2: (a) L1 in Al–1Mg alloy; (b) L2 in Al–5Mg alloy and (c) L3 in Al–9Mg alloy; the black lines show point-to-point misorientation, while the red lines show point-to-origin misorientation, respectively. (For interpretation of the references to colour in this figure legend, the reader is referred to the web version of this article.)

Fig. 4 shows the measured misorientation profiles along L1 -L3 in Fig. 3. Here, the black lines show point-to-point misorientation, while the red lines show point-to-origin misorientation, respectively.

As can be seen, the misorientation gradients in the coarse grains increased gradually with increasing Mg content, indicating the higher accumulation of dislocations. Furthermore, the dislocation

density of the HPRed samples can be estimated by measuring misorientation gradients in the coarse grains based on EBSD results [2,18,19]. The equivalent geometrically necessary dislocation density

can roughly be estimated by r z q/(bd), where q is the accumulated misorientation angle in radians within a distance d, and b is the Burgers vector. Taking b ¼ 2.86 □ 10□10 m for pure Al, with

values for q and d deriving from misorientation profiles in different grains in Fig. 4, the calculated results show the average dislocation density value increases from ~0.7 x $10^{14}m^{-2}$ in the Al-1Mg alloy to ~2 x $10^{14}m^{-2}$ in the Al-5Mg alloy and further to ~6 x $10^{14}m^{-2}$ in the Al-9Mg alloy. For comparison, the dislocation density has also been calculated by Williamson-Hall technique reported in Refs. [20,21], which is ~4.5 x $10^{14}m^{-2}$, ~11.8 x $10^{14}m^{-2}$ and ~46.4 x $10^{14}m^{-2}$ for the HPRed Ale1Mg, Al-5Mg and Al-9Mg alloys, respectively. Obviously, the dislocation density values calculated by Williamson-Hall technique are higher than those estimated from EBSD data. It is reasonable as the latter only provides density of geometrically necessary dislocation. Nevertheless, both dislocation density values calculated from XRD and EBSD data reflect the prominent role of Mg solutes for accumulation of a high dislocation density.

Fig. 5 shows representative TEM micrographs and corresponding grain size distributions of HPRed AleMg alloys. One can see that the microstructures consist of ultrafine grains (subgrains) and the

grain boundaries are fuzzy and ill-defined for all the three Al-Mg alloys. Fewer ultrafine grains with sizes <500 nm are observed in the Ale1Mg alloy (Fig. 5a and d), while, considerable amount of

equiaxed ultrafine grains in the size range ~200-400 nm are observed in the Al-5Mg and Al-9Mg alloys (Fig. 5b, e and c, f), in addition to elongated grains of ~200-1000 nm in length and~100-400 nm in width (Fig. 5c and e). The sizes of ultrafine grains in the HPRed Al-5Mg and Al-9Mg alloys are comparable to that (<~500 nm) in the ECAPed Al-7Mg alloy [2]. In addition, dislocation

tangle zones (DTZs) in grain interiors marked by white arrows become more evident with increasing Mg content, indicating an increased dislocation density.

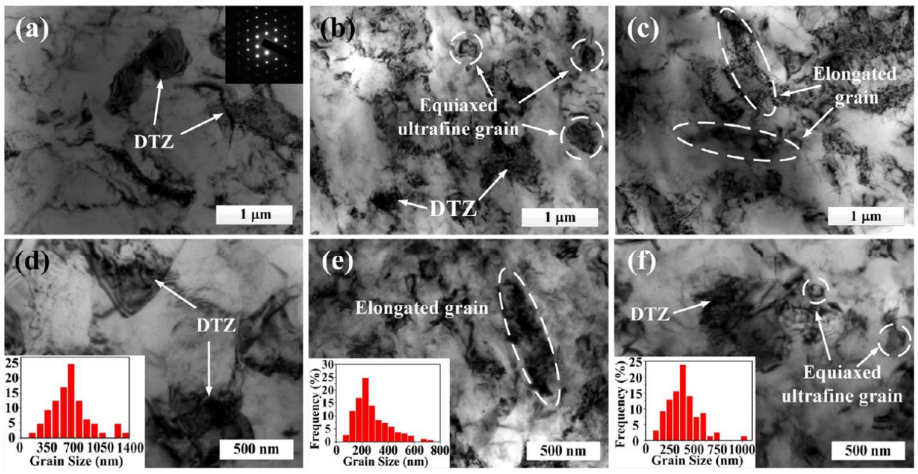

Fig. 5. Typical TEM images of the HPRed Al–Mg alloys: (a) (d) Al–1Mg, (b) (e) Al–5Mg and (c) (h) Al–9Mg alloys, respectively. The insertion in Fig. 5a is the corresponding diffraction pattern where typical reflexion of the Al phase indicates that no other precipitates formed.

Fig. 4 shows the measured misorientation profiles along L1–L3 in Fig. 3. Here, the black lines show point-to-point misorientation, while the red lines show point-to-origin misorientation, respectively. As can be seen, the misorientation gradients in the coarse grains increased gradually with increasing Mg content, indicating the higher accumulation of dislocations. Furthermore, the dislocation density of the HPRed samples can be estimated by measuring misorientation gradients in the coarse grains based on EBSD results [2,18,19]. The equivalent geometrically necessary dislocation density can roughly be estimated by $\rho \approx \theta/(b\delta)$, where θ is the accumulated misorientation angle in radians within a distance δ, and b is the Burgers vector. Taking $b = 2.86 \times 10^{-10}$ m for pure Al, with values for θ and δ deriving from misorientation profiles in different grains in Fig. 4, the calculated results show the average dislocation density value increases from ~0.7×10^{14} m^{-2} in the Al–1Mg alloy to ~2×10^{14} m^{-2} in the Al–5Mg alloy and further to ~6×10^{14} m^{-2} in the Al–9Mg alloy. For comparison, the dislocation density has also been calculated by Williamson-Hall technique reported in Refs. [20,21], which is ~4.5×10^{14} m^{-2}, ~11.8×10^{14} m^{-2} and ~46.4×10^{14} m^{-2} for the HPRed Al–1Mg, Al–5Mg and Al–9Mg alloys, respectively. Obviously, the dislocation density values calculated by Williamson-Hall technique are higher than those estimated from EBSD data. It is reasonable as the latter only provides density of geometrically necessary dislocation. Nevertheless, both dislocation density values calculated from XRD and EBSD data reflect the prominent role of Mg solutes for accumulation of a high dislocation density.

Fig. 5 shows representative TEM micrographs and corresponding grain size distributions of HPRed Al–Mg alloys. One can see that the microstructures consist of ultrafine grains (subgrains) and the grain boundaries are fuzzy and ill-defined for all the three Al–Mg alloys. Fewer ultrafine grains with sizes <500 nm are observed in

the Al–1Mg alloy (Fig. 5a and d), while, considerable amount of equiaxed ultrafine grains in the size range ~200–400 nm are observed in the Al–5Mg and Al–9Mg alloys (Fig. 5b, e and c, f), in addition to elongated grains of ~200–1000 nm in length and ~100–400 nm in width (Fig. 5c and e). The sizes of ultrafine grains in the HPRed Al–5Mg and Al–9Mg alloys are comparable to that (<~500 nm) in the ECAPed Al–7Mg alloy [2]. In addition, dislocation tangle zones (DTZs) in grain interiors marked by white arrows become more evident with increasing Mg content, indicating an increased dislocation density.

The collective information from EBSD and TEM results reveal that a bimodal grain structure consisting of a considerable fraction of micron sized grains mixed with some ultrafine grains forms in both the Al–5Mg and Al–9Mg alloys. A bimodal grain structure is known to be beneficial for the simultaneous increase in strength and ductility. Interestingly, it seems that more ultrafine (sub) grains are formed in the Al–5Mg alloy, as compared to Al–9Mg alloy, as seen from TEM observations and associated (sub) grain size distribution (Fig. 5). The increasing Mg solute content on one hand promotes a high dislocation density during HPR and provides higher driving force for dynamic recrystallization, meanwhile on the other hand it retards dislocation recovery which works in the opposite direction with respect to dynamic recrystallization. The microstructure evolution depends on the dynamic competition between the promoting and retarding effect of Mg solutes. More ultrafine grains are observed in the Al–5Mg alloy than in the Al–9Mg alloy indicates that fine recrystallized (sub) grains are more easier to form in the former. It is probably because that cross-slip or climb of dislocations associated with dynamic recovery is easier in the former, and hence (sub) ultrafine grains are more likely to form locally. In contrast, dislocation recovery may be effectively suppressed by the high level of solute Mg atoms in the Al–9Mg alloy, and hence the formation of sub grains is retarded while the dislocation density remains high. However, it is very difficult to form a dense 3D dislocation network to evolve into ultrafine grains in the Al–1Mg alloy due to the low dislocation density and fast dynamic recovery.

Consequently, the addition of Mg atoms to an Al matrix has significant effects on the microstructure evolution and hence mechanical properties of the HPRed Al–Mg alloys. On one hand, the increased Mg content in Al–Mg alloys can enhance the multiplication and accumulation of dislocations and meanwhile suppress dislocation recovery. On the other hand, the Mg solute atoms can act as obstacles to gliding dislocations, which have a strong effect on the strength. To further demonstrate the effect of Mg content on accumulation of high dislocation density and subsequent excellent mechanical properties, roles of various potential strengthening factors are evaluated.

It is well established that Mg atoms lead to solid solution strengthening ($\Delta\sigma_{ss}$) by decreasing the dislocation mobility, which is defined as follows:

$$\Delta\sigma_{ss} = HC^n \tag{1}$$

where C is the solute concentration (in wt.%); $H = 13.8$ (MPa/wt.%) and $n = 11.14$ were reported in Ref. [2]. Based on Eq. (1), the $\Delta\sigma_{ss}$ values for Al–1Mg, Al–5Mg and Al–9Mg alloys (~0.5, 5.0 and 7.2 wt.% Mg in HPRed Al–1Mg, Al–5Mg and Al–9Mg alloys, respectively) are estimated to be ~6.5 MPa, ~86 MPa and ~131 MPa, respectively.

The high dislocation density after HPR could provide significant contribution to the rapid increase in strength. The relationship between strength increment ($\Delta\sigma_D$) and dislocation density (ρ) in deformed metallic materials can be described by the Taylor equation:

$$\Delta\sigma_D = M\alpha_1 Gb\sqrt{\rho} \quad (2)$$

where $\alpha_1 = 0.3$ is a constant, $G = 27$ GPa is the shear modulus, $b = 2.86 \times 10^{-10}$ m is the length of the Burgers vector for Al and $M = 3$ the Taylor factor. Generally, for high Mg-containing Al–Mg alloys processed by SPD, the dislocation density is often estimated by measuring the misorientation profiles from EBSD maps [2]. Therefore, we applied the dislocation density estimated by EBSD results to consider strengthening contribution of dislocation density to YS for the HPRed Al–9Mg alloy in present work. The dislocation density applied here is ~0.7×10^{14} m^{-2}, ~2×10^{14} m^{-2} and ~6×10^{14} m^{-2} for Al–1Mg, Al–5Mg and Al–9Mg alloys, respectively, as estimated based on misorientation profiles from EBSD data. Therefore, the $\Delta\sigma_D$ for Al–1Mg, Al–5Mg and Al–9Mg alloys can be roughly calculated, i.e. ~56 MPa, ~98 MPa and ~170 MPa, respectively.

It is very difficult to calculate directly the strengthening contribution from grain boundaries as the HPRed high-Mg containing Al–Mg alloys have a very heterogeneous grain structure. Due to the total yield stress could be assumed to be a sum of various strengthening factors at the yield point, i.e.

$$\sigma_{YS} = \sigma_0 + \Delta\sigma_{SS} + \Delta\sigma_{GB} + \Delta\sigma_D \quad (3)$$

where σ_{YS} is the total yield stress, σ_0 refers to the crystal lattice friction, which is very low in face-centered cubic metals (such as Al) and hence can be neglected [22]. The yield strength values are ~150 MPa, ~240 MPa and ~355 MPa for Al–1Mg, Al–5Mg and Al–9Mg alloys, respectively. Hence the grain-boundary strengthening ($\Delta\sigma_{GB}$) contribution can be roughly estimated to be ~87 MPa, ~56 MPa and ~54 MPa, respectively.

In addition, the present HPRed Al–Mg alloys have much higher yield strength than that of the recrystallized Al–Mg alloys [9,23]. For instance, the present yield strength of Al–1Mg alloy (~150 MPa) and Al–5Mg alloy (~240 MPa) are about threefold higher than that of the recrystallized Al–1.05Mg alloy (~40 MPa) and Al–4.11Mg alloy (~75 MPa) [23]. From the true stress-strain curves showed in Fig. 1b, the work-hardening ability increases evidently with the solute Mg content. In fact, the effect of increasing Mg solutes on strength and ductility is similar to that of decreasing deformation temperature [23], i.e. the strength and work-hardening ability increase with higher Mg content or lower tension temperature."

The good ductility is mainly due to the strong work hardening ability that results from both the bimodal grain structure and the high Mg solute content. The addition of a high content of Mg solutes combined with the novel HPR technique favors greatly to the development of bimodal grain structures consisting of micron grains mixed with ultrafine grains (~200–400 nm). *E. Lavernia* et al. have reported that concurrent high ductility and strength can be obtained simultaneously in the bimodal grain structured Al–7.5Mg [24,25] and AA5083 Al [26] alloys. According to their study, the presence of ultrafine/nano grains in the microstructure are likely to contribute to the high strength via Hall-Petch mechanism, while the high ductility is attributed to the presence of coarse grains (~1 μm) which can suppress crack growth and thereby enhance ductility. In addition, the coarse grains have large dislocation storage capability and can accommodate relatively high density of dislocations. Furthermore, dislocations glide more easily in the coarse grains than in the ultrafine grains due to the former having a larger free slip pathway and fewer obstacles to dislocation slip [2]. Therefore, the coarse grains in the bimodal microstructure promote enhanced work-hardening ability and high ductility. Increasing Mg content in binary Al–Mg alloys strongly enhances the multiplication of mobile dislocations but decreases dislocation mobility, and

therefore benefits the work hardening. In addition, the DSA effect in Al−5Mg and Al−9Mg alloys is also beneficial for work hardening. In contrast, as compared to Al−5Mg and Al−9Mg, the largest proportion of low-angle boundaries formed in Al−1Mg are more effective sinks for dislocations, resulting in a reduced work hardening ability and thus a lower uniform ductility [27].

4. Conclusions

In summary, the new HPR was demonstrated to be an efficient and simple route in preparing high solid solution Mg content Al−Mg alloys. A bimodal microstructure consisting of coarse micron grains (>100 μm) and ultrafine grains (~200−400 nm) were formed in Al−5Mg and Al−9Mg alloys after HPR. Also, the HPRed Al−Mg alloys contain a high dislocation density, which increases dramatically with increasing Mg content. The HPRed Al−Mg alloys possess promising mechanical properties. Especially, the HPRed Al−9Mg alloy possesses a superior combination of high ductility (δ_f of ~14%) and strength (UTS of ~525 MPa). The high strength is mainly attributed to a high dislocation density, a high level of Mg solid solution and the ultrafine grains. The reason for the good ductility is the strong work hardening ability resulting from the bimodal grain structure and high Mg solute content. This work proposes a simple but efficient strategy to prepare hard-to-deform alloys with a good combination of strength and ductility.

References

[1] Y.-H. Zhao, X.-Z. Liao, S. Cheng, E. Ma, Y.T. Zhu, Simultaneously increasing the ductility and strength of nanostructured alloys, Adv. Mater. 18 (2006) 2280−2283.

[2] M. Zha, Y. Li, R.H. Mathiesen, R. Bjørge, H.J. Roven, Microstructure evolution and mechanical behavior of a binary Al-7Mg alloy processed by equal-channel angular pressing, Acta Mater. 84 (2015) 42−54.

[3] V.L. Niranjani, K.C. Hari Kumar, V. Subramanya Sarma, Development of high strength Al-Mg-Si AA6061 alloy through cold rolling and ageing, Mater. Sci. Eng. A 515 (2009) 169−174.

[4] S.K. Panigrahi, R. Jayaganthan, A study on the combined treatment of cryo-rolling, short-annealing, and aging for the development of ultrafine-grained Al 6063 alloy with enhanced strength and ductility, Metall. Mater. Trans. A Phys. Metall. Mater. Sci. 41 (2010) 2675−2690.

[5] W.S. Zhao, N.R. Tao, J.Y. Guo, Q.H. Lu, K. Lu, High density nano-scale twins in

Cu induced by dynamic plastic deformation, Scr. Mater. 53 (2005) 745–749.
[6] T. Shanmugasundaram, B.S. Murty, V. Subramanya Sarma, Development of ultrafine grained high strength Al-Cu alloy by cryorolling, Scr. Mater. 54 (2006) 2013–2017.
[7] Z. Horita, K. Ohashi, T. Fujita, K. Kaneko, T.G. Langdon, Achieving high strength and high ductility in precipitation-hardened alloys, Adv. Mater. 17 (2005) 1599–1602.
[8] X. Yang, D. Wang, Z. Wu, J. Yi, S. Ni, Y. Du, M. Song, A coupled EBSD/TEM study of the microstructural evolution of multi-axial compressed pure Al and Al-Mg alloy, Mater. Sci. Eng. A 658 (2016) 16–27.
[9] B.H. Lee, S.H. Kim, J.H. Park, H.W. Kim, J.C. Lee, Role of Mg in simultaneously improving the strength and ductility of Al-Mg alloys, Mater. Sci. Eng. A 657 (2016) 115–122.
[10] N. Tsuji, Y. Ito, Y. Saito, Y. Minamino, Strength and ductility of ultrafine grained aluminum and iron produced by ARB and annealing, Scr. Mater. 47 (2002) 893–899.
[11] H. Wang, Z. Yu, L. Zhang, C. Liu, M. Zha, C. Wang, Q. Jiang, Achieving high strength and high ductility in magnesium alloy using hard-plate rolling (HPR) process, Sci. Rep. 5 (2015) 17100.
[12] H. Ait-Amokhtar, C. Fressengeas, K. Bouabdallah, On the effects of the Mg content on the critical strain for the jerky flow of Al-Mg alloys, Mater. Sci. Eng. A 631 (2015) 209–213.
[13] R. Kaibyshev, E. Avtokratova, O. Sitdikov, Mechanical properties of an Al-Mg-Sc alloy subjected to intense plastic straining, Mater. Sci. Forum 638–642 (2010) 1952–1958.
[14] M. Zha, Y. Li, R.H. Mathiesen, R. Bjørge, H.J. Roven, Achieve high ductility and strength in an Al-Mg alloy by severe plastic deformation combined with inter-pass annealing, Mater. Sci. Eng. A 598 (2014) 141–146.
[15] X. Sauvage, N. Enikeev, R. Valiev, Y. Nasedkina, M. Murashkin, Atomic-scale analysis of the segregation and precipitation mechanisms in a severely deformed Al-Mg alloy, Acta Mater. 72 (2014) 125–136.
[16] Z. Horita, D.J. Smith, M. Furukawa, M. Nemoto, R.Z. Valiev, T.G. Langdon, An investigation of grain boundaries in submicrometer-grained Al-Mg solid solution alloys using high-resolution electron microscopy, J. Mater. Res. 11 (1996) 1880–1890.
[17] S. Jin, N. Tao, K. Marthinsen, Y. Li, Deformation of an Al-7Mg alloy with extensive structural micro-segregations during dynamic plastic deformation, Mater. Sci. Eng. A 628 (2015) 160–167.
[18] J. Gubicza, N.Q. Chinh, J.L. Lábár, S. Dobatkin, Z. Hegedus, T.G. Langdon, Correlation between microstructure and mechanical properties of severely deformed metals, J. Alloys Compd. 483 (2009) 271–274.
[19] M.P. Liu, H.J. Roven, M.Y. Murashkin, R.Z. Valiev, A. Kilmametov, Z. Zhang, Y. Yu, Structure and mechanical properties of nanostructured Al-Mg alloys processed by severe plastic deformation, J. Mater. Sci. 48 (2013) 4681–4688.
[20] Y.H. Zhao, X.Z. Liao, Z. Jin, R.Z. Valiev, Y.T. Zhu, Microstructures and mechanical properties of ultrafine grained 7075 Al alloy processed by ECAP and their evolutions during annealing, Acta Mater. 52 (2004) 4589–4599.
[21] G.K. Williamson, R.E. Smallman III, Dislocation densities in some annealed and cold-worked metals from measurements on the X-ray debye-scherrer spectrum, Philos. Mag. 1 (1956) 34–46.
[22] E.L. Huskins, B. Cao, K.T. Ramesh, Strengthening mechanisms in an Al-Mg alloy, Mater. Sci. Eng. A 527 (2010) 1292–1298.
[23] M. Jobba, R.K. Mishra, M. Niewczas, Flow stress and work-hardening behaviour of Al-Mg binary alloys, Int. J. Plast. 65 (2015) 43–60.
[24] D. Witkin, Z. Lee, R. Rodriguez, S. Nutt, E. Lavernia, Al-Mg alloy engineered with bimodal grain size for high strength and increased ductility, Scr. Mater. 49 (2003) 297–302.
[25] Z. Lee, D.B. Witkin, V. Radmilovic, E.J. Lavernia, S.R. Nutt, Bimodal microstructure and deformation of cryomilled bulk nanocrystalline Al-7.5Mg alloy, Mater. Sci. Eng. A 410–411 (2005) 462–467.
[26] A. Magee, L. Ladani, T.D. Topping, E.J. Lavernia, Effects of tensile test parameters on the mechanical properties of a bimodal Al-Mg alloy, Acta Mater. 60 (2012) 5838–5849.
[27] R. Kapoor, N. Kumar, R.S. Mishra, C.S. Huskamp, K.K. Sankaran, Influence of fraction of high angle boundaries on the mechanical behavior of an ultrafine grained Al-Mg alloy, Mater. Sci. Eng. A 527 (2010) 5246–5254.